ACS OMEGA

Open Access

http://pubs.acs.org/journal/acsodf

Article

Holistic Exploration of Structural, Electronic, Magnetic, Transport, Mechanical, and Thermodynamic Characteristics, Including Curie Temperature Analysis

Poorva Nayak,* Pankaj Srivastava, and Dinesh C. Gupta*

Cite This: *ACS Omega* 2023, 8, 48113−48129

Read Online

ACCESS | Metrics & More | Article Recommendations

ABSTRACT: Through intricate calculations, the density functional theory (DFT) implemented in the Wien2k code was employed to comprehensively investigate a wide range of material characteristics. Our study encompasses an exhaustive analysis of structural stability, electronic properties, magnetic behaviors, transport phenomena, mechanical responses, and thermodynamic profiles of two notable instances of filled Skutterudites, namely, $CeNi_4P_{12}$ and $DyCo_4Sb_{12}$, which have been thoroughly explored. These computations were performed using the WIEN 2K code, combining local orbitals and the full-potential linearized augmented plane-wave approach. The findings provided insight into the wide range of properties of these materials. In this methodology, the exchange−correlation potential relies on the local-density approximation. We conducted the calculations with and without incorporating spin−orbit interactions. The results obtained provide information about the lattice constant, bulk modulus, and pressure derivative. The stability, as indicated by the P−V graphical plot, suggests that there are no structural phase transitions from the cubic symmetry structure. Notably, our work includes an examination of Curie temperatures, which are pivotal in understanding magnetic phase transitions. The validated elastic properties further support the material's stability and corroborate its ductile nature. These alloys should be considered for spintronic and thermoelectric applications due to their estimated transport characteristics and the observed ductile nature. To enhance our understanding of the thermal stability of antimony-based compounds, we have made reliable estimations of the thermophysical characteristics. By integrating theoretical insights with practical implications, we bridge the gap between fundamental understanding and material design applications. Using DFT in the Wien2k framework, we discover connections and patterns among different properties, showing how to create materials with specific functions and better performance. This approach not only advances our fundamental comprehension of materials but also promises innovation across various technological domains.

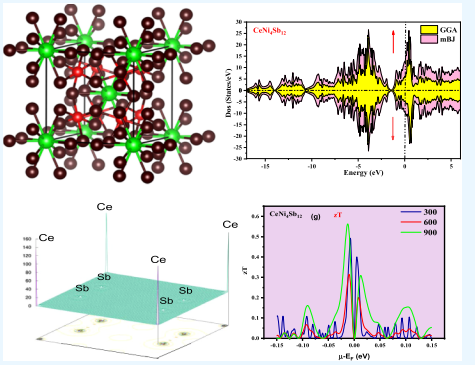

INTRODUCTION

The heat from waste materials can be directly converted into electricity by thermoelectric devices, which are expected to significantly contribute to future sustainable energy and power provision. A crucial requirement for the thermoelectric device's application is a high Seebeck coefficient (thermoelectric power), which is of utmost importance.[1,2] Skutterudite is a material of great interest in the field of thermoelectric and solid-state physics research. It belongs to the family of intermetallic compounds and is known for its exceptional thermoelectric properties. The unique crystal structure and composition of Skutterudites make them promising candidates for various energy conversion applications, including refrigeration, power generation, and energy harvesting. Moreover, Skutterudite has emerged as a solution for powering sensors and gadgets in the Internet of Things (IoT) era. Its ability to efficiently harvest waste and convert it into usable electrical energy offers new possibilities for self-powered and autonomous IoT devices, reducing the reliance on external power sources.[3,4] Skutterudites and Filled Skutterudites make up a group of substances characterized by their specific structural formulas: BC_3 and AB_4C_{12}, respectively. A (typically an infrequent or alkaline earth atom), B (a transition metal), and C (a pnictogen element). These substances showcase an extensive array of electronic characteristics, wherein their magnetic traits are shaped by solitary 3d and 4f electrons originating from the transition-metal B and rare-earth A constituents, respectively. Various intriguing phenomena have been observed in these compounds, including superconductivity,[5−7] semiconductivity,[8,9] magnetic order,[10−14] the behavior of heavy Fermion particles, valence fluctuation,,[15−17] and

Received: September 13, 2023
Revised: October 19, 2023
Accepted: November 8, 2023
Published: December 5, 2023

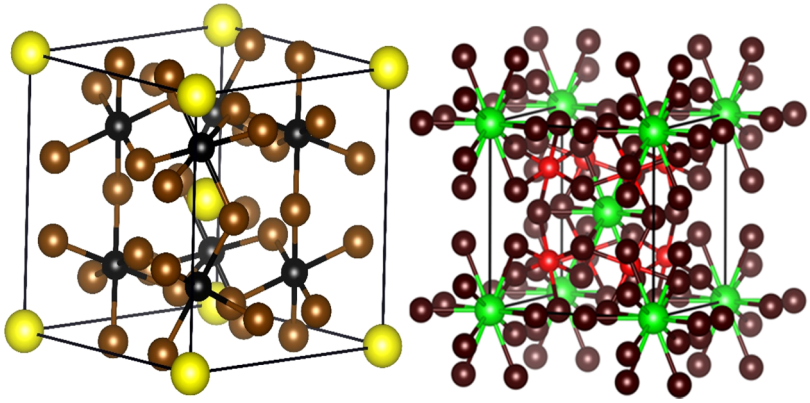

Figure 1. Perspective of the crystal structure of $CeNi_4Sb_{12}$ and $DyCo_4Sb_{12}$.

transition from conductive to insulating state.[18] These phenomena are often explained by valence fluctuations arising from the interaction between the localized f-electron states of the conduction electron state and the A ions. Such compounds typically exhibit elevated carrier mobility, reduced lattice thermal conductivity, and diminished electrical resistivity. These attributes position them as promising candidates for utilization in thermoelectric applications. In recent years, researchers have focused on improving the thermoelectric performance of Skutterudite through various methods. They have dedicated extensive research efforts to this goal. These include optimizing the composition and crystal structure, exploring new doping strategies, and improving the transport properties. These endeavors aim to further unlock the full potential of Skutterudites as a reliable and efficient thermoelectric material. In conclusion, Skutterudite has emerged as a promising thermoelectric material due to its unique crystal and impressive thermoelectric properties. Its high Seebeck coefficient and thermal stability make it an attractive candidate for converting waste heat into usable electricity. Ongoing research and development in this field continue to uncover new opportunities and advancements in harnessing Skutterudite's potential, including innovative materials design, enhanced manufacturing techniques, and novel thermoelectric device configurations. These developments pave the way for a more sustainable and energy-efficient future.

Theoretical Approach to Studying Computational Aspects. The Wien 2K package[19] utilizes the FPLAPW[20] technique to assess the properties of $CeNi_4Sb_{12}$ and $DyCo_4Sb_{12}$ compounds, including their structure, elasticity, and electronic characteristics. This code offers the capability to simulate various quantum mechanical properties, encompassing ground state structures, band gaps, and magnetic traits. In the initial stages, researchers employed various functional schemes, such as generalized gradient approximation (GGA),[21] and later GGA + mBJ,[22] to examine the electronic structures of skutterudite systems and evaluate their exchange−correlation potential (E_{Xc}). However, the accurate elucidation of the exchange−correlation aspect in the density functional theory (DFT) of complex many-body systems remains uncertain. Consequently, the generalized gradient approximation (GGA) was initially selected as an approximation to address the exchange−correlation potential. In the GGA formulation, E_{Xc} is treated as a derivative of the local charge density and its gradient. However, it has been frequently observed in previous studies that employing this approach explicitly for systems with d/f electrons fails to adequately represent the subsequent electronic structures. This deficiency not only leads to significant disparities in magnetic properties but also introduces various challenges associated with self-interaction errors. The self-interaction problem occurs when the artificial electron repulsion is not fully canceled, and there is no derivative discontinuity in the GGA functional. By including d/f electrons, we can use a pure ab initio approach to accurately refine their electronic structures. The modified Becke−Johnson (mBJ) potential is a technique that enables us to describe results with a high level of accuracy, even without experimental confirmation. It is a systematic method that allows us to make precise predictions based on theoretical calculations. This potential is particularly useful in situations where experimental data may be limited or unavailable. Therefore, utilizing this methodical potential approach is regarded as a preferable choice due to its ability to accurately portray outcomes prior to experimental results. The exchange−correlation potentials in this study were determined using the generalized gradient approximation (GGA) and modified Becke−Johnson (mBJ) approach. GGA is a method for approximating the exchange−correlation energy in density functional theory calculations. The modified Becke−Johnson method is an enhancement to GGA that improves the accuracy of the electronic structure calculations. These approaches were chosen to accurately describe the exchange and correlation effects between electrons in the system under investigation. To perform the Brillion zone integrations, a dense *k*-point mesh with dimensions of 10 × 10 × 10 was used. This means that the calculations considered many k-points in the Brillouin zone, which is a mathematical construct used to describe the behavior of electrons in a crystal lattice. The basic functions were expanded up to $R_{MT}K_{max} = 7$, where R_{MT} represents the smallest atomic cell and K_{max} corresponds to the magnitude of the largest K vectors in the plane-wave expansion. During the entire calculation process, the core and valence states were assigned numerical values of −7.0 R_y. The charge and energy were configured to values of 10^{-4} au^3 and 10^{-4} R_y, respectively. Furthermore, the cumulative charge difference between successive iterations remained under 10^{-4} au^3. In addition, the determination of elastic properties relied on the use of a specialized computational tool known as a "cubic elastic code" by Murtzamal.[23] This code was employed to accurately calculate and analyze the elastic properties, of the material, facilitating a precise characterization of its mechanical behavior. These elastic constants were then used to derive

https://doi.org/10.1021/acsomega.3c06694
ACS Omega 2023, 8, 48113−48129

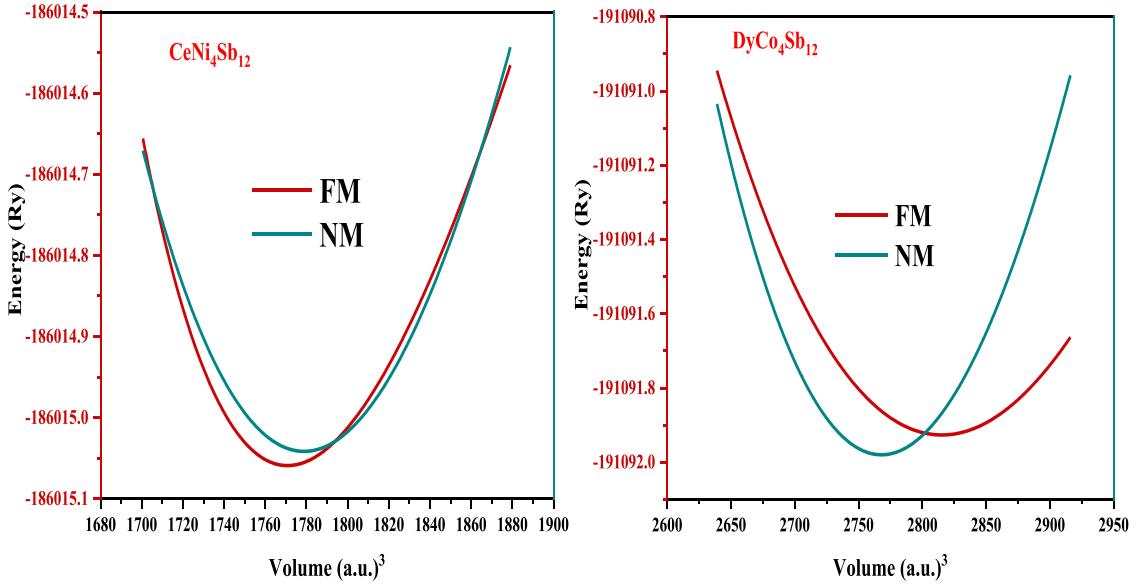

Figure 2. Plot depicting how the energy changes concerning the volume for $CeNi_4Sb_{12}$ and $DyCo_4Sb_{12}$.

Table 1. Parameters Extracted Including Equilibrium Lattice Constant *a* (in Å), Bulk Modulus (*B* in GPa), Bulk Modulus Derivative (B' in GPa), and Ground State Energies (E_0 in R_y) of $CeNi_4Sb_{12}$ and $DyCo_4Sb_{12}$

compounds	phases	*a* (Å)	*B*	B'	E (R_y)	*V*	E_{coh} (eV)
$CeNi_4Sb_{12}$	FM	8.07	4012.53	5.0	−185502.46	1979.81	4.10
	NM	8.24	5789.37	5.0	−185502.38	1778.81	
$DyCo_4Sb_{12}$	FM	8.21	2300.74	5.0	−191091.92	2851.26	3.09
	NM	8.47	1997.00	5.0	−191091.84	2693.63	
$Ce_{1.25}Fe_3CoSb_{12}$[32]		9.03[Exp]					
$CeFe_4Sb_{12}$[33]		9.14[Exp]					
$DyCo_4Sb_{12}$[34]		8.06[Exp]					
$Dy_{0.4}Co_4Sb_{12}$[35,36]		9.02[Exp]					

other mechanical parameters, allowing for a comprehensive analysis of the mechanical response exhibited by these materials. The BoltzTraP[24,25] scheme is a method we used to investigate the transport coefficient. It is based on the semiclassical Boltzmann theory and has been proven to be effective in analyzing and understanding electron transport behavior in materials. This scheme played a crucial role in our study and helped us achieve our research objectives. This approach allowed for exploration of the transport properties in the system. The investigation of thermodynamic properties has been conducted using the quasi-harmonic Debye model (Figure 1).[26,27]

RESULTS AND DISCUSSION

Crystal Structure and Stability of Magnetic Ground State. Skutterudite compounds having the general formula AB_4C_{12} (where A represents an alkali, alkaline, or rare-earth element; B represents Fe, Ru, or Os; and C represents P, As, or Sb) exhibit crystallization in the Skutterudite structure, which belongs to the Im3 space group. In the filled Skutterudite compounds $CeNi_4Sb_{12}$ and $DyCo_4Sb_{12}$, the atomic positions are arranged as follows: the Ce and Dy atoms occupy the coordinates (0,0,0), the Ni and Co atoms are located at (1/4,1/4,1/4), and the antimony atoms can be situated at (0,0.35,0.16). The positioning of the pnictogen element is established through the minimization of total energy while upholding a consistent volume as per experimental observations. In this study, the optimization process is achieved through the manipulation of internal parameters u and v. These parameters play a crucial role in attaining the desired energy and volume conditions necessary for arranging the specific pnictogen element within the material structure. This optimization process is essential for achieving the desired material properties and is a key aspect of our investigation. Through the optimization process, the values achieved for u and v were 0.3456 and 0.1546, respectively. By utilizing these optimized internal structural parameters, we can calculate the total energies for different lattice constant sets. Figure 2 depicts the connection between the minimum energies and the scaled volume. This visual representation highlights the alteration in the computed minimum energies as the volume is diminished. The Birch−Murnaghan equation of state[28] serves as a mathematical framework connecting total energies and lattice parameters. It offers a means to derive significant parameters such as the equilibrium lattice parameter lattice constant (a), bulk modulus (B_0), and the pressure derivative of the bulk modulus (B'). These parameters furnish valuable insights into the material's response under varying conditions. The significance of the difference between the computed and experimental values of the lattice constant lies in the comparison of these values. In the case of $CeNi_4Sb_{12}$, the computed lattice constant is 8.07, while the experimental value is 8.0497, showing a difference of approximately 1.4%. For $DyCo_4Sb_{12}$, the computed lattice constant is 8.21, again with a small difference compared with the experimental value. This

https://doi.org/10.1021/acsomega.3c06694
ACS Omega 2023, 8, 48113−48129

difference is important because it indicates how well the computational model aligns with real-world observations. Moreover, it is predicted that at a pressure of zero, the bulk modulus (B_0) and pressure derivative of bulk modulus (B') will amount to 240.52 GPa and 5.21, respectively. The values calculated (226.716 GPa and 6.72) are like those acquired through an X-ray diffraction investigation.[29] The calculated lattice parameters like lattice constant a (in Å), bulk modulus (B in GPa), bulk modulus derivative (B' in GPa), and ground state energies (E_0 in R_y) of $CeNi_4Sb_{12}$ and $DyCo_4Sb_{12}$ are represented in Table 1. Figure 1 shows the crystal structures of $CeNi_4Sb_{12}$ and $DyCo_4Sb_{12}$. The predicted values of B_0 and B' are important because they provide information about the mechanical properties of $CeNi_4Sb_{12}$ and $DyCo_4Sb_{12}$. The bulk modulus (B_0) is a measure of a material's resistance to compression, and the pressure derivative of bulk modulus (B') is a measure of how the material's resistance to compression changes with pressure. A high bulk modulus indicates that a material is difficult to compress, and a high-pressure derivative of bulk modulus indicates that the material's resistance to compression increases rapidly with pressure. The assessment of the chemical stability and practical feasibility of the suggested compounds $CeNi_4Sb_{12}$ and $DyCo_4Sb_{12}$ involves an analysis of two critical factors: formation energy (E_{For}) and cohesive energy (E_{Coh}). E_{For}, or formation energy, represents the energy required for creating each unit of the compound. Researchers use this value to gauge the compound's energetic favorability. A lower E_{For} value suggests a higher likelihood of spontaneous formation and increased stability. On the other hand, E_{Coh}, or cohesive energy, denotes the energy necessary to hold the atoms within the compound together. A compound with high E_{Coh} demonstrates strong atomic bonding, leading to increased stability. To conduct these assessments, researchers employ specialized mathematical equations or formulas tailored to the unique properties and characteristics of the elements comprising the compound. These equations allow for the quantitative determination of E_{For} and E_{Coh}, providing valuable insights into the compound's overall stability and practical feasibility (Table 2).[30]

$$E_{For} = (E_{Ce}^{bulk} + E_{Ni}^{bulk} + E_{Sb}^{bulk}) - E_{CeNi_4Sb_{12}}^{total}$$

$$E_{For} = (E_{Dy}^{bulk} + E_{Co}^{bulk} + E_{Sb}^{bulk}) - E_{DyCo_4Sb_{12}}^{total}$$

$$E_{Coh} = (E_{Ce}^{iso} + E_{Ni}^{iso} + E_{Sb}^{iso}) - E_{CeNi_4Sb_{12}}^{total}$$

$$E_{Coh} = (E_{Dy}^{iso} + E_{Co}^{iso} + E_{Sb}^{iso}) - E_{DyCo_4Sb_{12}}^{total}$$

E_{Ce}^{bulk}, E_{Ni}^{bulk}, E_{Dy}^{bulk}, E_{Co}^{bulk}, and E_{Sb}^{bulk} correspond to the energies of the Ce, Ni, Dy, Co, and Sb atoms in their bulk form, with these values determined by estimating the energies of bulk atoms in free space. On the other hand, E_{Ce}^{iso}, E_{Ni}^{iso}, E_{Dy}^{iso}, E_{Co}^{iso}, and E_{Sb}^{iso} represent the isolated atomic energies of the constituent atoms.

Table 2. Total Magnetic Moment of $CeNi_4Sb_{12}$ and $DyCo_4Sb_{12}$ under Both the Generalized Gradient Approximation (GGA) and GGA + mBJ Approximations

compounds	methods	magnetic moment (μB)
$CeNi_4Sb_{12}$	GGA	3.62
	GGA + mBJ	5.61
$DyCo_4Sb_{12}$	GGA	4.06
	GGA + mBJ	6.12

Additionally, we use $E_{CeNi_4Sb_{12}}^{total}$ and $E_{DyCo_4Sb_{12}}^{total}$ energies of $CeNi_4Sb_{12}$ and $DyCo_4Sb_{12}$, respectively, to describe the total energy per formula unit of the $CeNi_4Sb_{12}$ and $DyCo_4Sb_{12}$ compounds. The negative values of the formation energies for $CeNi_4Sb_{12}$ and $DyCo_4Sb_{12}$ indicate that it is a stable compound that is feasible to synthesize in the laboratory. The cohesive energy, which is a measure of the strength of the bonds between the atoms in a compound, is also substantial for $CeNi_4Sb_{12}$ and $DyCo_4Sb_{12}$. This suggests that the compound is chemically stable and that the constituent atoms are strongly bonded together. The compounds' stability is assessed by considering the enthalpy energy, represented as ΔE. This value is determined through the following formula:[31]

$$\Delta H = E_{total} - aE_A - bE_B - xE_X$$

The overall energies of the $CeNi_4Sb_{12}$ and $DyCo_4Sb_{12}$ compounds are denoted by E_{total}. Ce, Ni, and X, and Dy, Co, and X are represented by E_A, E_B, and E_X, respectively. The calculated energy values for $CeNi_4Sb_{12}$ and $DyCo_4Sb_{12}$ are −5.63 and −4.21 R_y, respectively. These negative values of the enthalpy of formation energy indicate that the compounds are stable. The calculated values of cohesive, formation, and enthalpy energies are given in Table 3.

Table 3. Estimated Values of the Cohesive Energy (E_{coh} in eV/Atom), Formation Energy (E Formation in eV/Atom), and Enthalpy (R_y)

compound	E_{coh} (eV/atom)	$E_{formation}$ (eV/atom)	enthalpy (R_y)
$CoNi_4Sb_{12}$	4.10	−0.34	−5.63
$DyCo_4Sb_{12}$	3.09	−0.41	−4.21

Electronic Properties. To investigate the spin-polarized electronic properties of $CeNi_4Sb_{12}$ and $DyCo_4Sb_{12}$ Skutterudite compounds, we performed a comprehensive analysis of their electronic band structure and density of states (DOS). To ensure accuracy, we employed two distinct exchange−correlation schemes and took into account the relaxed lattice constants for both compounds. Exploring the electronic properties of two-dimensional materials offers several advantages. These materials have unique properties due to their atomic thickness such as high carrier mobility, tunability, and strong quantum confinement effects. These properties make them suitable for various applications, including electronics, optoelectronics, energy storage, and sensing. By studying the electronic behavior of these materials, researchers can gain insight into fundamental physics and develop new devices with improved performance and functionality. Overall, the exploration of two-dimensional materials' electronic properties has wide-ranging implications in many research fields. In this context, we utilized both PBE-GGA and GGA + mBJ schemes to examine and envisage the characteristics such as band structure and the corresponding density of states for the innovative $CeNi_4Sb_{12}$ and $DyCo_4Sb_{12}$ compounds. The outcome of this analysis, depicted in Figure 3, provides valuable insights. Most importantly, our analysis employing GGA reveals a significant observation pertaining to $CeNi_4Sb_{12}$ and $DyCo_4Sb_{12}$. Specifically, the energy bands within the spin-up channels exhibit a tangential contact near the Fermi energy level (E_F), with crossing it. This distinct behavior indicates that $CeNi_4Sb_{12}$ possesses metallic properties, with a zero forbidden band gap. Similarly, in the spin-down channel of both $CeNi_4Sb_{12}$, we observe a similar metallic nature, characterized

https://doi.org/10.1021/acsomega.3c06694
ACS Omega 2023, 8, 48113−48129

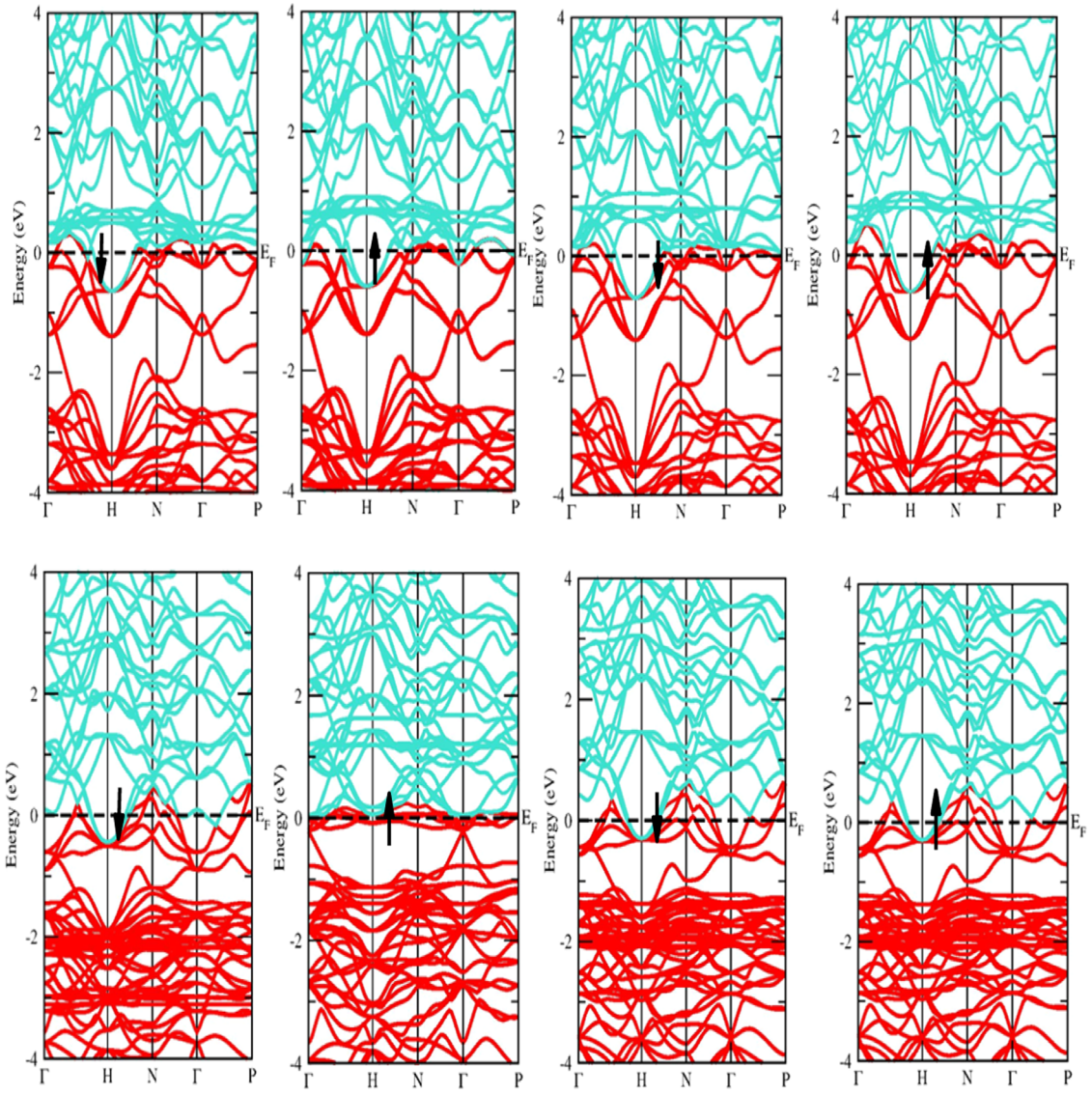

Figure 3. Computed band structures of CeNi4Sb12 and DyCo4Sb12, depicted across the high-symmetry pathway within the first Brillouin zone using the GGA and GGA + mBJ scheme.

by a zero-band gap. This implies that as we transition from the spin-up to the spin-down pathway, the band gap of these materials exhibits a slight decrease owing to the symmetrical behavior of the corresponding band structures. In contrast, when considering the compound $DyCo_4Sb_{12}$ under the same analysis, it demonstrates a preference for a metallic nature within this applied scheme, characterized by a zero band gap value. Nonetheless, it is of utmost importance to emphasize and consider that the prominent use of the GGA potential in systems where d-electrons are already present carriers is an inherent limitation when accurately interpreting their electronic band profiles. Therefore, caution must be exercised when interpreting the electronic band profiles of these materials using GGA. To address this uncertainty, an alternative approach using the DFT formulation involves utilizing the mBJ potential, which is based on the *ab initio* calculations. The TB-mBJ correlation scheme was specifically calibrated to provide a more accurate representation of the electronic structure in Skutterudites. By incorporating the TB-mBJ correlation scheme, it becomes evident that the metallic electronic band structures remain preserved in the cubic lattice structure of $CeNi_4Sb_{12}$ and $DyCo_4Sb_{12}$, albeit with a zero-band gap. The transition from GGA to mBJ clearly clarifies the genuine metallic behavior of these systems. This interpretation is reinforced by the examination of the total density of states (TDOS), atomic contribution, and partial density of states (pDOS), as illustrated in Figures 4−6, respectively.

The TDOS results obtained using both the GGA and mBj approximation scheme align with the previously discussed observations, as represented in Figure 4. Additionally, the pDOS analysis enables a detailed investigation of the orbital contributions from atoms in different states, as shown in Figure 6. This unveils noticeable energy gaps between states mainly arising from the valence and conduction bands surrounding the reference level within $CeNi_4Sb_{12}$ and $DyCo_4Sb_{12}$. These gaps are illustrated through the advanced functional representation provided by the mBJ scheme.

These findings are significant because they confirm the metallic nature of the filled compounds, which is a fundamental characteristic of their electronic properties. The use of the "advanced mBJ scheme" adds to the understanding of these materials by providing a more precise and accurate

https://doi.org/10.1021/acsomega.3c06694
ACS Omega 2023, 8, 48113−48129

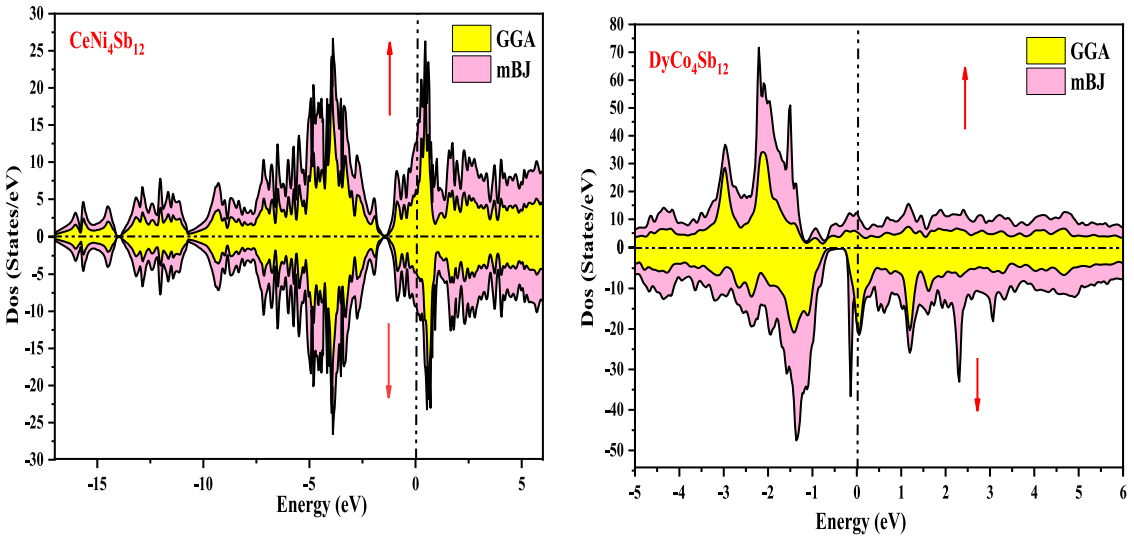

Figure 4. DFT calculations performed by harnessing the PBE-GGA and TB-mBJ functionals to determine the total density of states (TDOS) for $CeNi_4Sb_{12}$ and $DyCo_4Sb_{12}$.

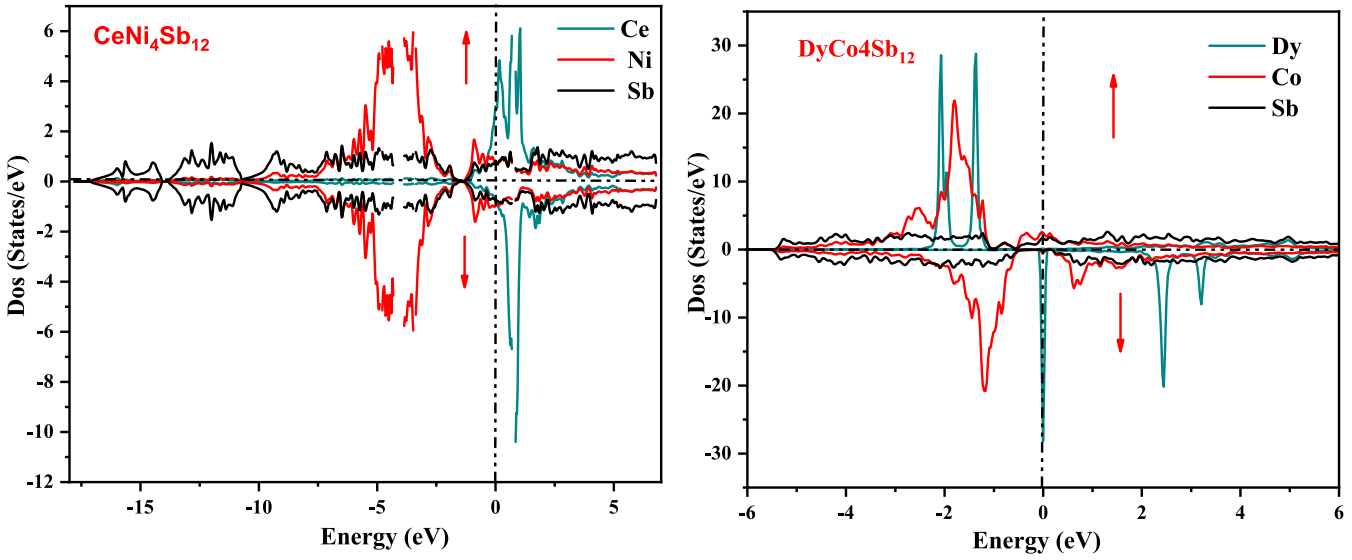

Figure 5. Leveraging the GGA + mBJ approach, atomic contribution to band formation for $CeNi_4Sb_{12}$ and $DyCo_4Sb_{12}$.

description of their electronic structure. This advanced scheme offers improved accuracy in calculating electronic properties, allowing for better characterization of the metallic behavior in these compounds. Furthermore, the consistency of these results with previous studies on related compound series[33,34] strengthens the understanding of the materials' electronic properties, making it a valuable contribution to the field of materials science. This provides compelling evidence that this chemical system indeed demonstrates metallic behavior. Furthermore, the consistency observed among the resulting band structures and the total and partial density of states further strengthen the similarity in these materials.

Curie Temperature and Magnetic Properties. Determining the Curie temperature $T_C = \Delta E/3k_B$ for these compounds was done using a specific equation within the framework of the Heisenberg model, as discussed in refs 37,38. In this equation, ΔE represents the energy difference, calculated as ENM (the total energy of the nonmagnetic state) minus EFM (the total energy of the ferromagnetic state) for both CeNi4Sb12 and DyCo4Sb12 substances. The Boltzmann constant (k_B) is also a part of this equation. By calculating ΔE, we are essentially quantifying the energy barrier that needs to be overcome for this transition to occur. When TC is reached, the thermal energy available at that temperature becomes sufficient to disrupt the ferromagnetic alignment of the magnetic moments within the material. So, the difference in total energies (ΔE) between the nonmagnetic and ferromagnetic states is crucial for determining TC because it tells us at what temperature the material's magnetic properties are expected to change. It helps us understand the thermal energy required to influence the magnetic behavior of these substances, making it a key parameter in the study of their magnetic properties and phase transitions. Based on these calculations, the foretold curie temperature values are 422 and 390 K for $CeNi_4Sb_{12}$ and $DyCo_4Sb_{12}$, respectively. It is noteworthy that the assessed value for T_c of $CeNi_4Sb_{12}$ and $DyCo_4Sb_{12}$ is lower than that at room temperature, indicating their suitability for applications requiring lower temperatures.

In this ongoing scrutiny, the materials $CeNi_4Sb_{12}$ and $DyCo_4Sb_{12}$, which are based on rare-earth elements, have

https://doi.org/10.1021/acsomega.3c06694
ACS Omega 2023, 8, 48113−48129

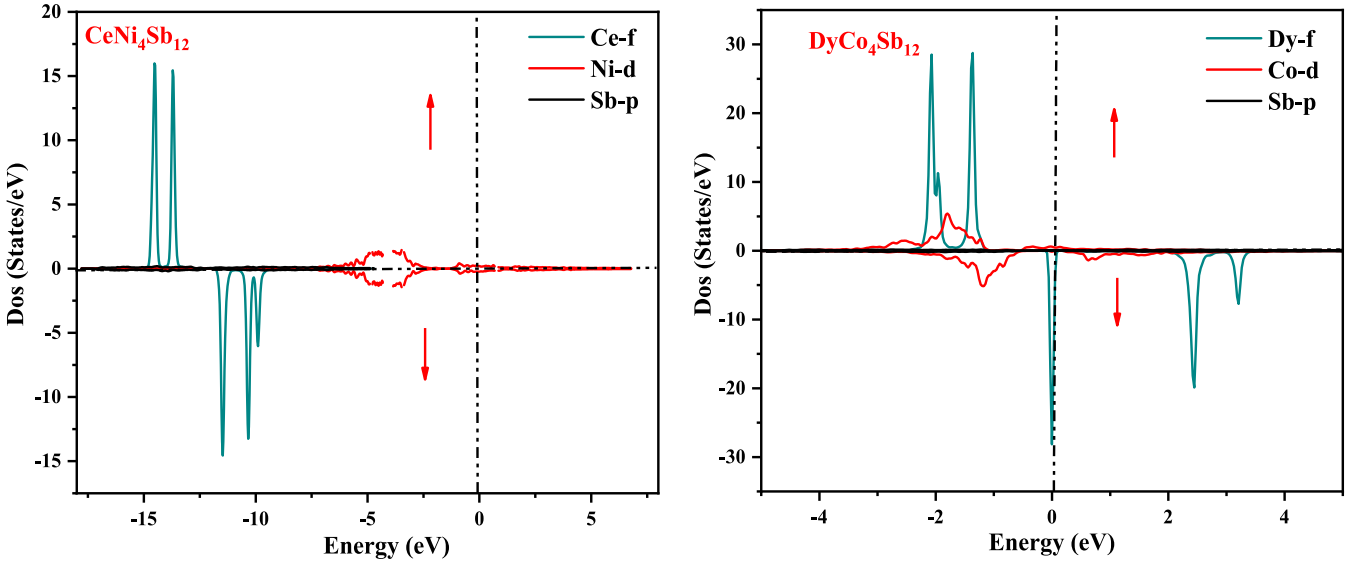

Figure 6. DFT calculations to obtain the partial density of states (pDOS) for $CeNi_4Sb_{12}$ using the mBJ exchange−correlation function. Additionally, DFT calculations were performed to acquire pDOS for $DyCo_4Sb_{12}$ by using the mBJ exchange−correlation functional.

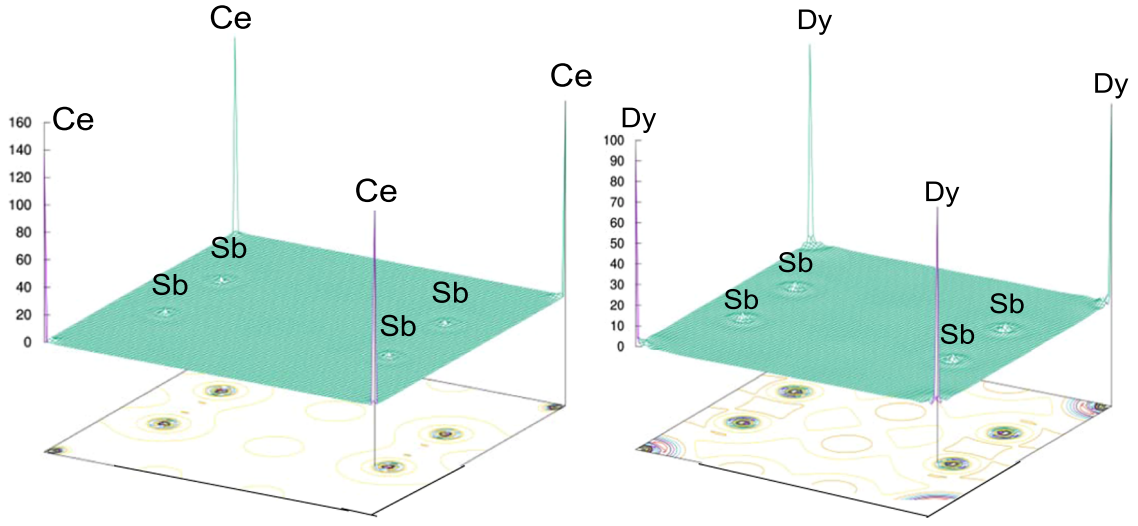

Figure 7. Electron charge density plot in the (110) plane for $CeNi_4Sb_{12}$ and $DyCo_4Sb_{12}$ unveils the distribution of electron densities within these crystal structures.

attracted special interest. These materials possess inherent magnetism within their lattice structures, making them a promising candidate for spintronics applications. The magnetism of these representative-filled Skutterudites was analyzed by using the simulation process of Wien 2K with GGA and GGA + mBJ approximations, as indicated in Table 2. By employing these approximations schemes, it was observed that the entire spin magnetic moment, rather than the orbital magnetic moment, in $CeNi_4Sb_{12}$ and $DyCo_4Sb_{12}$ Skutterduite, is approximately 5.61 and 6.12 μB, respectively, which aligns well with previously reported values. Furthermore, a meticulous analysis was conducted to discern the distinct contributions of individual atoms within their lattice configuration. As depicted in Table 2, it becomes evident that the dominant magnetism is chiefly influenced by Ce in $CeNi_4Sb_{12}$ and Dy in $DyCo_4Sb_{12}$. The Ce-f and Dy-f energy states represent the electronic energy levels of the cerium (Ce) and dysprosium (Dy) atoms, respectively. These energy levels are localized, meaning that the electrons in these states are confined to a small region around the nucleus. This observation aligns with the prevalence of energy states Ce-f and Dy-f, which are predominantly localized in proximity to the reference level. The localization of the Ce-f and Dy-f energy states is significant because it allows these atoms to exhibit unique magnetic and electronic properties. For instance, Ce and Dy are both ferromagnetic, meaning that they have spontaneous magnetization. This is because the electrons in the Ce-f and Dy-f energy states can align their spins in a parallel fashion. The localization of the Ce-f and Dy-f energy states is also important for applications in quantum computing and spintronics. The observation that the energy states Ce-f and Dy-f are predominantly localized in the proximity of the reference level is significant because it helps to explain the prevalence of these energy states. The reference level is the theoretical energy level that represents the energy of an electron at rest. The fact that the Ce-f and Dy-f energy states are localized in proximity to the reference level means that they are relatively low in energy. This makes them more

https://doi.org/10.1021/acsomega.3c06694
ACS Omega 2023, 8, 48113−48129

likely to be occupied by electrons, which explains why they are so prevalent. Conversely, the magnetism exhibited by other constituent atoms, namely, Ni, Co, and Sb in both structural instances, remains relatively feeble due to their inherent paramagnetic characteristics. Paramagnetic compounds are characterized by symmetric electronic band structures, thus showcasing magnetic properties solely under the influence of an externally applied magnetic field.[39,40] The magnetic moment's positive and negative values signify ferromagnetic and antiferromagnetic−ferrimagnetic interactions among the diverse components within the lattice structures. In fact, the observed magnetism within these specified compounds is attributed to the indirect exchange interaction between neighboring Ce and Dy atoms facilitated by nonmagnetic atoms Sb. This exchange mechanism encompasses both double-exchange and superexchange interactions. Generally, double-exchange promotes ferromagnetism, while super-exchange favors antiferromagnetism. In our scenario, the spin magnetic moment emerging from the periodic lattice arrangements amplifies their potential for utilization in spintronics, magnonics, and allied fields. The observed spin magnetic moment resulting from the periodic lattice arrangements has significant implications for applications in spintronics, magnetics, and related fields. This magnetic moment amplifies the potential of these materials for use in such applications. In spintronics, it enables precise manipulation and control of electron spins, which can be harnessed for developing advanced electronic devices such as spin-based transistors and memory storage systems. In magnonics, the spin magnetic moment enhances the generation and propagation of magnons, which are collective excitations of electron spins. This can lead to the development of efficient magnonics devices for data transfer and processing. Overall, the presence of a spin magnetic moment in these materials opens exciting possibilities for innovations in spintronics, magnetonics, and related technologies.

Electronic Charge Density. In addition, the charge densities of $CeNi_4Sb_{12}$ and $DyCo_4Sb_{12}$ Skutterudites system along the (110) plane were computed and presented in Figure 7, expressed in the units of eÅ^3. The arrangement of electronic charges surrounding the individual atoms within the lattice offers valuable insights into their interplay and the characteristics of chemical bonding. Analysis of the electron density plots clearly reveals that the interaction between Ce and Sb, as well as Dy and Sb atoms in their respective compounds, exhibits a metallic nature. Moreover, the degree of metallic nature in the latter situation increases on the order of decreasing electronegativity. The metallic nature of these bonds finds additional affirmation through the heightened values and the occurrence of d−d hybridization within these substances. The contour lines exhibited in Figure 7 further elucidate the potency and scope of covalent bonding within this framework. Conversely, the bonding interactions concerning Ce−Sb and Dy−Sb manifest a distinctly metallic essence, devoid of any covalent participation. The term "metallic essence" refers to the nature of the chemical bonding that is characteristic of metals. Metallic bonding is a type of chemical bonding that occurs in metals and is characterized by the delocalization of electrons across a lattice of positively charged metal ions. This delocalization of electrons results in a unique set of properties commonly associated with metals, such as electrical conductivity, malleability, ductility, and the ability to form metallic lattices with strong metallic bonds.

Mechanical Properties. Understanding the elasticity of materials is crucial for comprehending their mechanical properties and making them valuable for various industries and technology applications. Elastic properties describe a material's ability to resist deformation in size and shape when subjected to external forces. This process is reversible, meaning that the material can return to its original state after deformation, particularly under small deformations where linear elasticity applies and stress−strain relationships are linear. However, when materials experience large deformations, they may undergo permanent changes. "Permanent changes" refer to alterations or modifications in the material's structure or properties that persist even after the deforming force or stress has been removed. These changes are not reversible and represent a lasting transformation in the material's state. In practical terms, this could include changes in shape, size, or mechanical properties, such as increased hardness, altered electrical conductivity, or modified thermal properties, which remain even when the material is no longer under the influence of external force or deformation. The term permanent changes highlights that these alterations are not temporary and have a lasting impact on the material's behavior and characteristics. In the case of $CeNi_4Sb_{12}$ and $DyCo_4Sb_{12}$ materials, the elastic constants are determined through initial computational assessments employing density functional theory (DFT). This involves accurately relaxing the material′s structure to a nearly stress-free state. The cubic elastic package incorporated within Wien 2K has been employed for this specific purpose.[41] The cubic elastic package is a powerful tool that utilizes density functional theory (DFT) calculations to simulate the behavior of atoms in a crystal lattice under mechanical strains. It enables researchers to study how the energy of the crystal changes with different types of strains. By analyzing these energy changes and using mathematical techniques, the package can determine elastic constants, which are crucial for predicting the deformation of a material under different mechanical loads. This package provides valuable insights into the mechanical properties of materials and aids in the design of materials with specific desired characteristics. The determination of elastic constants is contingent upon the material's symmetry with cubic systems requiring solely three autonomous second-order elastic parameters: C_{11}, C_{12}, and C_{44}. These parameters serve to define the material's resilience. C_{11} corresponds to longitudinal compression and correlates with the material hardness. C_{12} elucidates transverse distortion, intricately linked to Poisson's ratio and influenced by the cation present on the B-site. C_{44} defines the shear modulus. The computed data set, found in Table 2, unequivocally illustrates that all of the measured second-order stiffness tensors C_{ij}, expressed in GPa, are positive. This substantiates the indisputable elastic stability of the materials and adheres to the stability criteria posited by the generalized Born Huang conditions.[42,43] Derived from the stipulated elastic tensor conditions: $C_{11} > 0$, $C_{12} > 0$, $C_{44} > 0$, $C_{11} + 2C_{12} > 0$, $C_{11} - C_{12} > 0$, $C_{44} > 0$, various comprehensive elastic modulus like Bulk modulus (B), Young's modulus (Y), and shear modulus (G) can be computationally determined. The bulk modulus measures a material's resistance to a change in volume when subjected to an external pressure. It is defined as the ratio of the change in pressure (ΔP) to the fractional change in volume ($\Delta V/V$). Bulk modulus is critical in understanding how materials respond to compression or expansion. It is particularly relevant in applications like hydraulic systems, where fluids are compressed, and in

https://doi.org/10.1021/acsomega.3c06694
ACS Omega 2023, 8, 48113−48129

designing materials that need to withstand high-pressure environments, such as pressure vessels and hydraulic systems. Young's modulus measures a material's ability to resist deformation under an axial or tensile load. It quantifies the ratio of stress (force per unit area) to strain (change in length per unit length) in the direction of the applied load. Young's modulus is crucial for designing and selecting materials in applications where tensile or compressive forces are involved. For example, it helps engineers choose the right materials for structural components in buildings, bridges, and aerospace. High Young's modulus materials deform less under a given load, making them suitable for load-bearing structures. The shear modulus, also known as the modulus of rigidity, measures a material's resistance to shear deformation. It quantifies the ratio of shear stress to shear strain in a material. Shear modulus is crucial in situations where materials experience forces that cause them to slide or deform without changing their volume. It is used in designing materials for applications like the construction of foundations, earthquake-resistant buildings, and mechanical systems where materials must withstand shear forces. Consequently, an assessment of the material's properties concerning its ductility or brittleness can be ascertained by evaluating parameters such as the Pugh ratio (B/G), Poisson's ratio (υ), Zener's anisotropy (A), and Cauchy's pressure (C_p).

$$B_V = B_G B = \frac{C_{11} + 2C_{12}}{3} G_v$$

$$G_R = \frac{5(C_{11} - C_{12})C_{44}}{4C_{44} + 3(C_{11} + C_{12})},\ G_v = \frac{C_{11} - C_{12} + 3C_{44}}{5}$$

$$Y = \frac{9BG}{3B + G};\ \sigma = \frac{3B - 2G}{2(3B + G)};\ \upsilon = \frac{3B - Y}{6B}$$

$$A = \frac{2C_{44}}{C_{11} - C_{12}} \text{ and } C_P = C_{12} - C_{44}$$

The examination of specific parameters can be succinctly categorized into subsequent subsections. The Bulk modulus (B) delineates the compounds' resistance to alterations in volume brought about by external pressure, reflecting their compressibility. A comparison of the calculated bulk modulus values highlights a notable disparity between $CeNi_4Sb_{12}$ and $DyCo_4Sb_{12}$. Evidently, $CeNi_4Sb_{12}$ exhibits a significantly more pronounced volumetric change in contrast to that of $DyCo_4Sb_{12}$, suggesting a greater compressibility in the former. Moreover, a significant characteristic encompasses the Young modulus (Y), which assumes pivotal importance in industrial and aerospace engineering domains. This modulus governs the material's adaptability across diverse applications. Likewise, the shear modulus (G) quantifies the materials' capacity to endure transverse deformation. Furthermore, the materials' tendencies toward ductility or brittleness can be anticipated through the evaluation of Pugh's ratio (B/G).[44] The pivotal threshold for the bulk modulus/shear modulus ratio (B/G) is 1.75. A material surpassing this value is categorized as ductile, while a value below 1.75 denotes brittleness. Within the context of the examined compounds, a B/G value of 0.99 suggests brittleness, whereas a value of 0.84 signifies brittle behavior. Poisson's ratio (υ),[45] another parameter of note, contributes to predicting a material's ductility or brittleness. The determined values for Poisson's ratio, namely, 0.12 and 0.07, point toward a comparable character for both alloys. In the same vein, Cauchy's pressure (C_p)[46] is assessed, with its outcome signifying the materials' brittle or ductile disposition. For $CeNi_4Sb_{12}$, a negative C_p value denotes brittleness, while the negative C_p value for $DyCo_4Sb_{12}$ indicates a brittleness behavior. Zener's anisotropic factor (A)[47] serves to disclose whether the compounds exhibit isotropic or anisotropic traits. An A value of unity signifies pure isotropy, implying uniform properties in all directions. The acquired A values for both compounds surpass unity, indicating their anisotropic nature. Furthermore, the melting temperature (T_m),[48] a fundamental thermodynamic measure, holds significance in this context.

$$T_m = [553(K) + (5.911)C_{11}]GPa \pm 300\ K$$

This is computed using a conventional equation. The resulting T_m values stand at 2559.46 and 2247.42 K for the corresponding compounds. These figures signify the preservation of lattice configurations and imply that these alloys do not undergo phase alterations. In essence, these recorded values furnish compelling substantiation for the pragmatic application of these alloys across diverse engineering and industrial contexts. Furthermore, they affirm the viability of the experimental production of these materials. These outcomes find reinforcement through the annotated values displayed in Table 4. Table 4 represents the calculated value of the elastic constant bulk modulus (B), shear modulus (G), and Young's modulus (Y), all expressed in gigapascals (GPa). Additionally, the calculations encompassed the melting temperature (T_m), Poisson's ratio (υ), anisotropy constant (A), Cauchy pressure (C_p), and Pugh's ratio (B/G).

Table 4. Subsequent Parameters of Compounds $CeNi_4Sb_{12}$ and $DyCo_4Sb_{12}$, Elastic Constants (C_{ij} in GPa), Bulk Modulus (B in GPa), Shear Modulus (G in GPa), and Young's Modulus (Y in GPa), All Expressed in Gigapascals (GPa)[a]

	compounds	
parameters	$CeNi_4Sb_{12}$	$DyCo_4Sb_{12}$
C_{11}	433	380.21
C_{12}	59	60.34
C_{44}	183	225.56
C_p	−124	−165.22
B	183.66	166.96
Y	414.80	423.45
Gv	184.60	199.31
G_R	184.57	193.75
G	184.58	196.53
υ	0.12	0.07
B/G	0.99	0.84
A	1.97	1.41
T_m	2559.46	2247.42

[a]Additionally, the calculations encompassed the melting temperature (T_m) in Kelvin (K), Poisson's ratio (υ), anisotropy constant (A), Cauchy pressure (C'' in GPa), and Pugh's ratio (B/G).

Thermodynamic Properties. Additionally, to assess the thermodynamic stability of the examined compound and its suitability for device fabrication, various thermodynamic parameters have been calculated. These parameters include volume (V), heat capacity (C_V), Grüneisen constant (γ), Debye temperature (θ), entropy (S), and thermal expansion coefficient (α). This analysis specifically applies to compounds $CeNi_4Sb_{12}$ and $DyCo_4Sb_{12}$. Heat capacity quantifies the energy

https://doi.org/10.1021/acsomega.3c06694
ACS Omega 2023, 8, 48113−48129

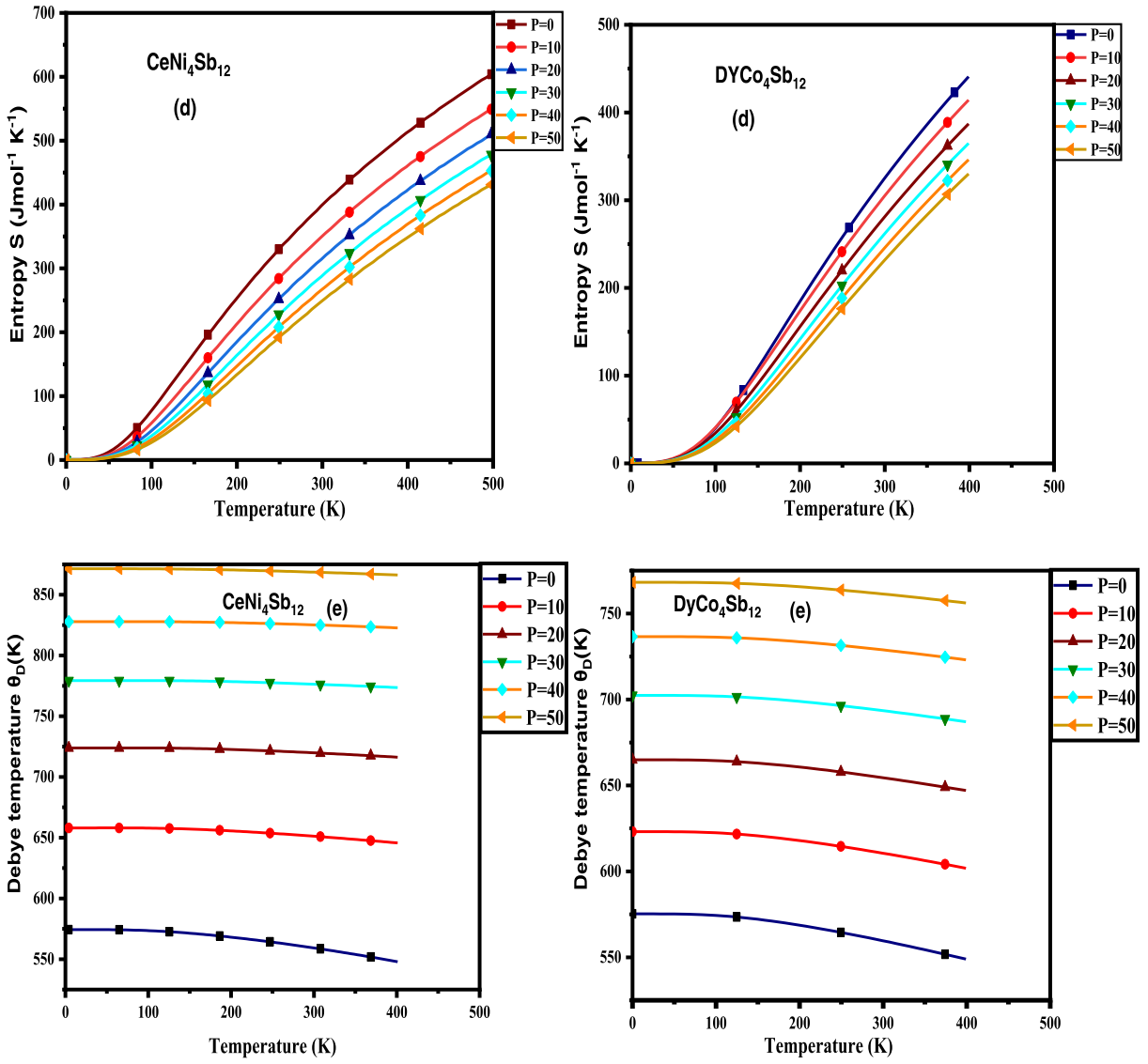

Figure 8. (a) Temperature-related fluctuations in the heat capacity (α). (b) Temperature-induced changes in Grüneisen constant (γ). (c) Temperature-linked fluctuations in thermal expansion coefficient (α). (d) Temperature-driven fluctuations in entropy (S). (e) Temperature-induced variations in the Debye temperature (θ_D).

needed to raise or lower the temperature of a substance with a given mass by a certain amount. It imparts valuable insights into the lattice vibrational and phase transition behavior. The figure indicates that at lower temperatures, the heat capacity (C_V) experiences a rapid increase, primarily driven by the prevalence of an anharmonic effect in accordance with the T^3 law of the Debye model. Within the temperature range of 0−500 K, the nature of the heat capacity is characterized as logical as shown in Figure 8a. However, at higher temperatures, the influence of anharmonicity is diminished, leading to the achievement of the saturation limit known as the Dulong−Petit limit.[49] This phenomenon can be attributed to the thermal energy leading to the excitation of phonon modes within the substance. Conversely, the heat capacity (C_V) shows a decreasing trend with increasing pressure across all of the examined temperature values. The nature of the heat capacity of $CeNi_4Sb_{12}$ and $DyCo_4Sb_{12}$ Skutterudites adheres to the Debye model. At 300 K and 0 GPa, the calculated values for these Skutterudites are 377.8734 kJ mol^{-1} for $CeNi_4Sb_{12}$ and 361.5431 kJ mol^{-1} for $DyCo_4Sb_{12}$. The Dulong−Petit limit, characterized by the maximum heat capacity, is attained by $CeNi_4Sb_{12}$, and $DyCo_4Sb_{12}$ at 300 K and 0 GPa. The data provided here may assist experimentalists seeking to gather information about heat capacity (C_V).

To comprehend the nature of the Grüneisen constant (γ), its variation with temperature (T) and pressure (P) is depicted in Figure 8b for $CeNi_4Sb_{12}$ and $DyCo_4Sb_{12}$. The Grüneisen constant (γ) is a parameter that signifies the alteration in vibrational frequency when a material is subjected to elevated temperature and pressure. Consequently, these changes in temperature and pressure influence the dynamics of the crystal. The Grüneisen constant (γ) is a parameter that represents how the vibrational frequencies of atoms in a material change when it is exposed to higher temperatures and pressures. This constant is significant because it provides insights into how a material's internal structure responds to changing environmental conditions. Specifically, increasing the temperature causes atoms in the material to vibrate more vigorously. The Grüneisen constant quantifies how these vibrations change with temperature, which is crucial in fields such as thermal

https://doi.org/10.1021/acsomega.3c06694
ACS Omega 2023, 8, 48113−48129

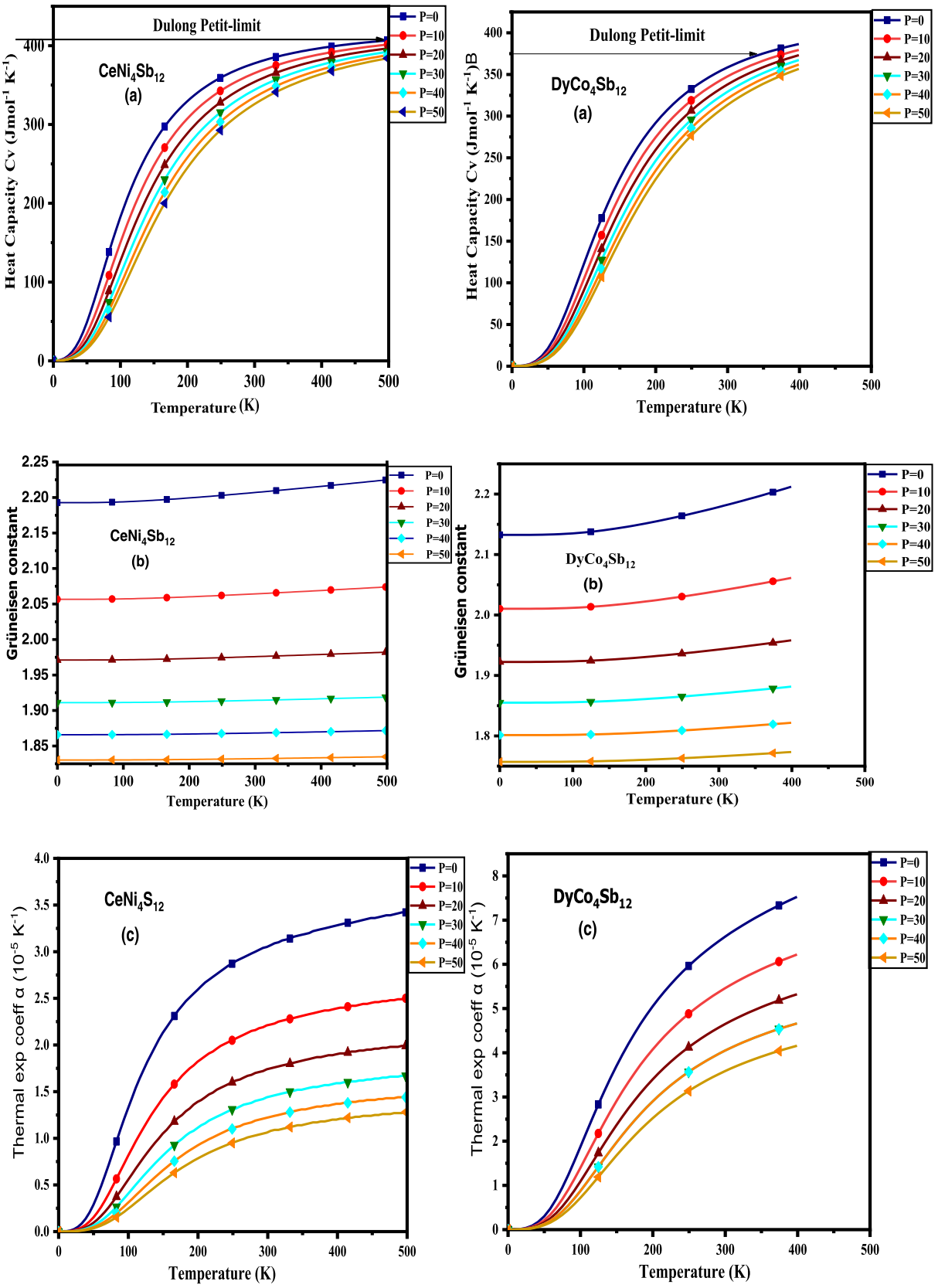

conductivity, where it affects how heat is conducted through the material. Elevated pressure can compress the spacing between the atoms in the material. The Grüneisen constant helps us to determine how this compression affects the material's vibrational frequencies. This knowledge is valuable in high-pressure physics, where it is important to predict how materials behave under extreme pressure conditions. The Grüneisen constant plays a vital role in understanding the thermal expansion and phase transitions. It tells us how the material responds to changes in temperature and pressure,

https://doi.org/10.1021/acsomega.3c06694
ACS Omega 2023, 8, 48113−48129

Table 5. Presents Thermodynamic Data for $CeNi_4Sb_{12}$ and $DyCo_4Sb_{12}$ Materials at Room Temperature under Various Pressure Conditions (P in GPa)

material	P (GPa)	C_V (kJ mol^{-1})	γ	α (10^{-5} K^{-1})	θ_D (K)	S (J mol^{-1} K^{-1})
$CeNi_4Sb_{12}$	0	377.8734	2.20738	3.07	559.28	405
	10	366.6215	2.06446	2.22	651.26	356
	20	355.7363	1.97599	1.75	719.9	321
	30	345.8319	1.91441	1.45	776.4	294
	40	336.6911	1.86835	1.23	825.21	272
	50	328.1744	1.83221	1.08	868.63	254
$DyCo_4Sb_{12}$	0	361.5431	2.18104	6.71	470.92	334
	10	351.1115	2.04144	5.53	537.03	314
	20	341.7744	1.94403	4.71	591.9	289
	30	333.2608	1.87098	4.11	639.62	270
	40	325.4017	1.81351	4.11	682.3	253
	50	318.0823	1.76672	3.64	721.2	239

helping us predict when phase transitions might occur and how materials will expand or contract with temperature changes. The variation of the Grüneisen constant with the temperature and pressure is important because it helps us understand how a material expands or contracts and how its thermal and mechanical properties change in response to these factors. Figure 8b illustrates a gradual increase in the value of γ as the temperature ranges from 0 to 500 K while maintaining constant pressure values of 0, 10, 20, 30, 40, and 50 GPa. Our findings indicate that the Grüneisen constant experiences a rapid decrease as the pressure increases while maintaining constant temperature values. The influence of pressure on $CeNi_4Sb_{12}$ and $DyCo_4Sb_{12}$ Skutterudites is found to be more pronounced compared to temperature. The obtained Grüneisen constants at 300 K temperature and zero pressure for $CeNi_4Sb_{12}$ and $DyCo_4Sb_{12}$ are 2.20738, and 2.18104, respectively.

Figure 8c displays the volumetric thermal expansion coefficient (α) relative to the temperature (T) and pressure (P). These plots provide insight into the expansion of substance in all directions when subjected to heat. This expansion occurs due to the movement of the constituent particles within the substance. The graphical representation indicates that the α value exhibits a rapid rise until 100 K, after which a gradual and incremental rise is observed. At standard room temperature and pressure (0 GPa), the recorded α values for $CeNi_4Sb_{12}$ and $DyCo_4Sb_{12}$ are 3.07×10^{-5} and 6.71×10^{-5} K^{-1}, respectively. Interestingly, with increasing pressure, these values exhibit an opposite effect compared with the influence of temperature. An ongoing decrease in α is evident as the pressure changes while maintaining a constant temperature. The highest value of α is observed at the lowest pressure range. The α parameter is also useful in assessing the nature of the bonding within solids. A smaller value of α indicates stronger bonding, while a larger value suggests weaker bonding. This study delves into the systematic understanding of the thermal properties of $CeNi_4Sb_{12}$ and $DyCo_4Sb_{12}$ Skutterduite, laying the foundation for future experimental investigations in this field. The volumetric thermal expansion coefficient (α) is highly relevant in materials science and engineering due to its role in predicting and managing the material response to temperature changes. This parameter helps engineers and scientists understand how a material's volume will change as it heats or cools, which is crucial for designing structures and systems that can withstand thermal variations without deformation or failure. By selecting materials with compatible thermal expansion coefficients, engineers can ensure dimensional stability in applications ranging from buildings to aerospace components.

Entropy (S) provides valuable insight into uncertainty and disorder within a system. By examining the changes that arise from temperature and pressure variations, we can gain insight into the extent of randomness or disruption within the materials. Figure 8d depicts the graphical representation of entropy (S) concerning temperature (T) in the range of 0−700 K and pressure (P) spanning from 0 to 50 GPa, focusing on $CeNi_4Sb_{12}$ and $DyCo_4Sb_{12}$ Skutterudites. These illustrations highlight that entropy reaches zero at absolute zero temperature (0 K) and at a pressure of zero the entropy (S) exhibits an exponential increase with temperature (T), indicating that at higher temperatures, there is an increased level of disturbance within the material at constant pressure. On the other hand, with increasing pressure, the disturbance and disorder within the material decrease, implying a higher level of order. Although temperature encourages thermal vibrations, pressure tends to mitigate these oscillations. In this context, entropy-temperature graphical representation, no discontinuity in the entropy values was observed, indicating the absence of phase transitions. For $CeNi_4Sb_{12}$ and $DyCo_4Sb_{12}$ Skutterudite at 0 GPa and 300 K, the reported entropy values are 405 and 334 J mol^{-1} K^{-1}, respectively.

The Debye temperature (θ_D) is a valuable indicator of the thermoelastic properties, particularly in gauging material hardness. Materials boasting a higher θ_D exhibit a relatively stiffer nature when compared to compounds with lower θ_D values. The temperature-dependent behavior of θ_D is graphically depicted in Figure 8e, revealing a noticeable decrease in θ_D as the temperature rises. At lower temperatures, the impact of thermal expansion and anharmonicity remains minimal, resulting in an almost constant Debye temperature. Even high-frequency modes can be regarded as effectively immobilized at these lower temperature ranges. Furthermore, an increase in the pressure correlates with an elevation in θ_D. This phenomenon is attributed to the heightened atomic bonding that occurs under increased pressure conditions. Table 5 provides data on the room temperature value of θ_D. The notably high Debye temperature values in these materials suggest their potential suitability for applications even at elevated temperatures.

Thermoelectric Properties. The thermoelectric coefficients were computed utilizing the semiclassical Boltzmann transport theory as outlined in refs 25,50, and these

https://doi.org/10.1021/acsomega.3c06694
ACS Omega 2023, 8, 48113−48129

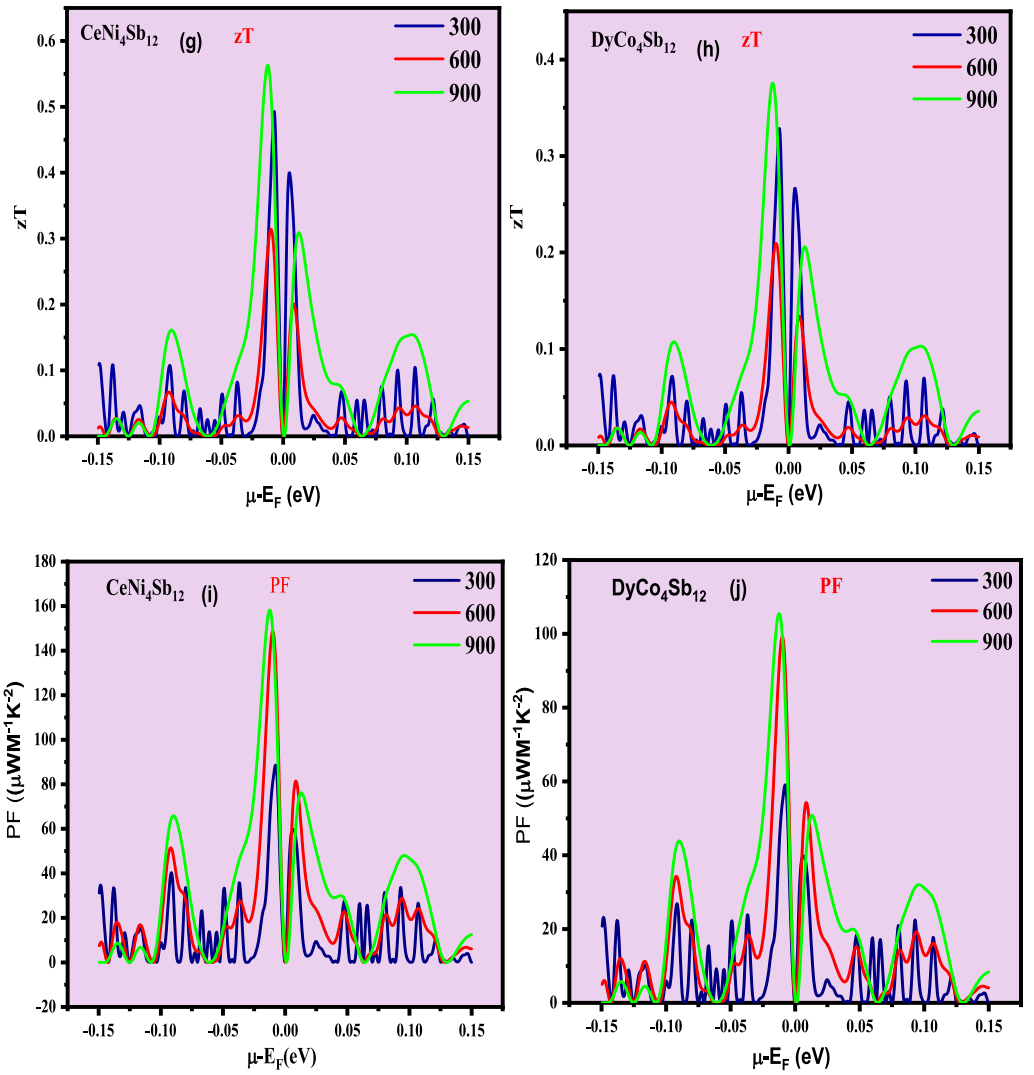

Figure 9. Graphs illustrating the dependence of (a, b) Seebeck coefficient (S), (c, d) electrical conductivity (σ/τ), (e, f) electronic thermal conductivity (κe), (g, h) figure of merit (zT), and (i, j) power factor on the chemical potential for $CeNi_4Sb_{12}$ and $DyCo_4Sb_{12}$. To distinguish between temperatures, different colors have been employed: Blue represents 300 K, red represents 600 K, and green represents 900 K.

calculations were executed using the BoltzTraP software. The semiclassical Boltzmann transport theory is used to compute thermoelectric coefficients by considering how electrons move in response to both electrical and thermal gradients within the material. This theory provides a fundamental understanding of how charge carriers scatter and interact with the crystal lattice, impurities, and other carriers. These calculations are essential for designing and engineering efficient thermoelectric materials, as they guide the selection of materials and their structural configurations to maximize the thermoelectric efficiency. BoltzTraP software is a widely used computational tool that employs this theory to perform these calculations, helping researchers design and optimize thermoelectric materials for various applications. This software provides a trustworthy and effective numerical approach for deriving analytical expressions while accommodating the limitations associated with the relaxation time constant (τ). Through a comprehensive investigation of transport parameters encompassing the Seebeck coefficient (S), electrical conductivity (σ/τ), thermal conductivity (κ), figure of merit (zT), and power factor (PF), the thermoelectric efficacy of materials such as $CeNi_4Sb_{12}$ and $DyCo_4Sb_{12}$ was precisely evaluated. This evaluation involved a meticulous analysis of how these parameters behave in relation to the chemical potential (μ) across three distinct temperatures (300, 600, and 900 K). The classification of n-type and p-type regions is determined by the polarity of μ, where positive values denote p-type and negative values indicate n-type. The insight into these two Skutterudites systems is facilitated by examining the Seebeck coefficient (S), as illustrated in Figure 9a,b. This representation reveals distinct peaks and valleys across the entire spectrum of the chemical potential, conveying noteworthy variations in the graph. The visualization aptly portrays alternating high-intensity peaks for both positive and negative potentials at 600 K. Nonetheless, with the escalation of the temperature, the prominence of these peaks gradually diminishes. The driving force behind this phenomenon lies in the fact that elevated temperatures energize bound electrons through thermal absorption, leading to the creation of electron−hole pairs. The most notable peaks emerge within the energy range of 0−0.05 eV, a consequence of the less dispersive nature of bands in this interval, consequently creating a forbidden zone around the Fermi level. This, in turn, results in a reduced presence of charge carriers within this energy span. At a temperature of 300 K, $CeNi_4Sb_{12}$ exhibits a

https://doi.org/10.1021/acsomega.3c06694
ACS Omega 2023, 8, 48113−48129

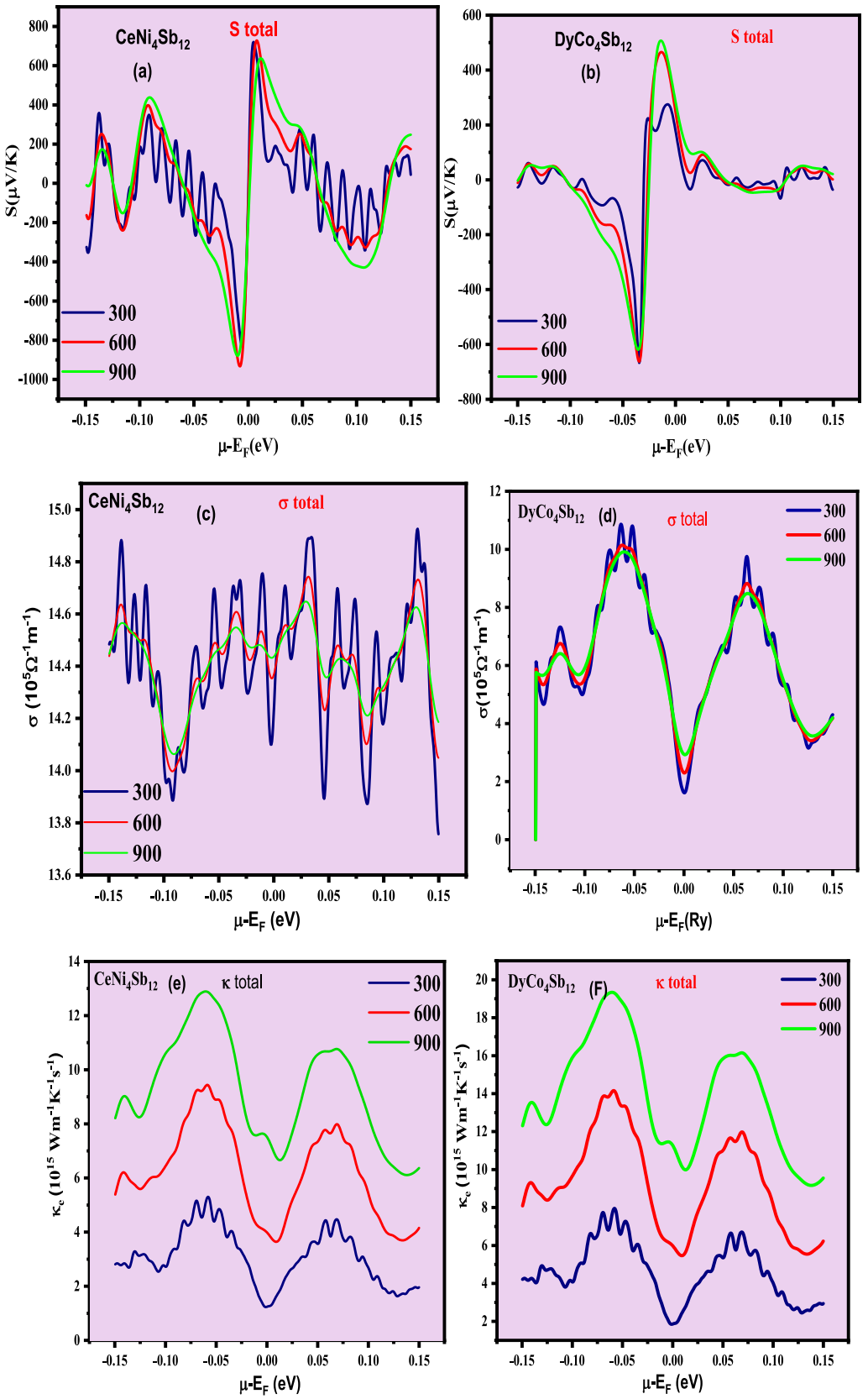

peak Seebeck coefficient (S) value of 800 μV K^{-1}, whereas $DyCo_4Sb_{12}$ displays a slightly lower value of 700 μV K^{-1}. These findings enable the deduction that $CeNi_4Sb_{12}$ demonstrates a substantially elevated Seebeck coefficient. This can be attributed to its zero band gap and the highly correlated nature of localized f-bands, which contribute to boosted thermoelectric properties. It has been noted that a multitude of rare-earth compounds, wherein the f-level closely aligns with the Fermi energy, manifest notably substantial Seebeck coefficients. This phenomenon can be attributed to

https://doi.org/10.1021/acsomega.3c06694
ACS Omega 2023, 8, 48113−48129

the narrowness of the f-bands in these materials, which results in a significantly heightened density of states proximate to the Fermi level. As a result, the temperature-dependent Seebeck coefficient of such substances reveals distinct voltages in both the spin-up and spin-down channels, owing to their possession of metallic attributes. This distinctive attribute bestows the metallic unit cell with inherent thermocouple characteristics. Consequently, in the presence of a temperature gradient, this configuration generates propelling forces in line with their corresponding spin orientations, giving rise to the emergence of the spin-Seebeck effect. Consequently, our investigation delved into the correlation between the alteration of electrical conductivity concerning relaxation time (σ/τ) and the chemical potential at three distinct temperatures, considering the reliance on the chemical potential. The conductive behavior of the two Skutterudite compounds, namely, $CeNi_4Sb_{12}$ and $DyCo_4Sb_{12}$, is vividly illustrated in Figure 9c,d. This graph illustrates variations in electrical conductivity in response to alterations in the chemical potential. As the chemical potential varies within a specific range, typically between −0.15 and 0.15, there are observable changes in electrical conductivity. These variations can be attributed to shifts in the population of charge carriers within the material. When the chemical potential falls within this range, certain energy bands near the Fermi level are populated, leading to enhanced electrical conductivity. Conversely, when the chemical potential is outside this interval, the conductivity tends to decrease as fewer charge carriers are available. Furthermore, we also examine the behavior of electronic thermal conductivity (κ_e) in relation to changes in the chemical potential, as illustrated in Figure 9e,f. This visual representation highlights how alterations in the chemical potential impact the electronic thermal conductivity. When the chemical potential shifts, electrons within the material acquire varying levels of thermal energy. This, in turn, affects their ability to contribute to heat conduction. As the chemical potential changes, the electronic thermal conductivity may increase or decrease depending on the availability of thermally excited electrons for conduction. In conclusion, the intrinsic parameters have been compiled to determine the zT value of $CeNi_4Sb_{12}$ and $DyCo_4Sb_{12}$, as illustrated in Figure 8g,h. The presence of distinct peaks in these values, approaching unity (1), signifies their promising potential in energy harvesting, nanoengineering, and applications, such as radioisotope generator systems (RTG). In RTG setups, the decay energy of a radioactive material is harnessed through a series of thermocouples interconnected in a cascade configuration, converting this energy back into a usable electrical form and leveraging the principle of the Seebeck effect. We also examine the behavior of the power factor (PF) in relation to changes in the chemical potential, as illustrated in Figure 9i,j. The power factor (PF) in metallic compounds is a critical parameter for evaluating their thermoelectric performance. It quantifies the material's ability to effectively convert heat into electrical power when exposed to a temperature gradient. Computed as PF = $(S\wedge 2 \times \sigma)/\kappa$, it relies on the Seebeck coefficient (S), electrical conductivity (σ), and electrical resistivity (ρ). A high power factor signifies superior thermoelectric efficiency, achieved when a substantial Seebeck coefficient generates a significant voltage, high electrical conductivity facilitates efficient charge transport, and low electrical resistivity minimizes energy losses. Such compounds hold promise for thermoelectric applications, such as waste heat recovery and solid-state cooling, where optimizing thermal-to-electrical energy conversion is crucial. Researchers are actively working to identify materials with enhanced power factors to advance sustainable energy technologies and enhance the energy conversion efficiency.

CONCLUSIONS

In summary, our comprehensive investigation encompassing structural, electronic, magnetic, thermoelectric, and thermophysical properties and Curie temperature of $CeNi_4Sb_{12}$ and $DyCo_4Sb_{12}$ has provided a holistic understanding of these materials. The analysis of their crystal structures revealed distinctive arrangements that directly influence their electronic and transport behaviors. In rare-earth compounds such as $CeNi_4Sb_{12}$ and $DyCo_4Sb_{12}$, the proximity of the f-level to the Fermi energy results in significant Seebeck coefficients due to their tightly packed f-bands and many states near the Fermi level. These compounds exhibit metallic characteristics that give rise to captivating spin-dependent phenomena, as observed in the spin-Seebeck effect. Moreover, our analysis of their electronic attributes emphasizes the intricate interaction between the f-level and Fermi energy, playing a pivotal role in shaping their electrical conductivity and conductive behaviors. The magnetic exploration yielded valuable information about the compounds' magnetic interactions and Curie temperatures. This understanding is crucial for harnessing their magnetic properties for applications in areas such as data storage and magnetic devices. The thermoelectric investigations underscored the potential of these metallic compounds for thermoelectric applications. The determination of parameters such as the Seebeck coefficient and electronic thermal conductivity illuminated their ability to convert temperature gradients into electrical voltage, making them promising candidates for energy harvesting and waste heat recovery. Furthermore, the evaluation of thermophysical properties provided insights into the compounds' heat transport characteristics, which are vital for applications involving heat conduction and dissipation. To sum up, our exhaustive investigation into the structural, electronic, magnetic, Curie temperature, thermoelectric, and thermophysical attributes of $CeNi_4Sb_{12}$ and $DyCo_4Sb_{12}$ in their metallic forms not only deepens our understanding of these materials but also opens avenues for their potential utilization in various technological sectors. Skutterudite materials offer exciting prospects for improving the energy efficiency across diverse applications. One particularly compelling application involves transforming the waste heat generated by vehicle exhaust systems into electricity, which can then be redirected to power the vehicle itself. This innovation allows for recharging of the vehicle's batteries, leading to decreased reliance on traditional fuels and fostering a greener, more sustainable approach to transportation. The potential applications of these materials are thermoelectric generators to convert waste heat into electricity and thermoelectric coolers to generate cooling from electricity

AUTHOR INFORMATION

Corresponding Authors

Poorva Nayak − *Condensed Matter Theory Group, School of Studies in Physics, Jiwaji University, Gwalior 474001, India;* orcid.org/0000-0002-3527-009X; Email: poorvanayak11@gmail.com

https://doi.org/10.1021/acsomega.3c06694
ACS Omega 2023, 8, 48113−48129

Dinesh C. Gupta − *Condensed Matter Theory Group, School of Studies in Physics, Jiwaji University, Gwalior 474001, India*; Email: sosfizix@gmail.com

Author

Pankaj Srivastava − *Atal Bihari Vajpayee Indian Institute of Information Technology and Management, Gwalior 474015, India*

Complete contact information is available at: https://pubs.acs.org/10.1021/acsomega.3c06694

Notes

The authors declare no competing financial interest.

■ ACKNOWLEDGMENTS

The authors sincerely thank Jiwaji University Gwalior for providing the necessary facilities to conduct this research. No financial support has been provided for this research work.

■ REFERENCES

(1) Slack, G. A.; Tsoukala, V. G. Some properties of semiconducting IrSb3. *J. Appl. Phys.* **1994**, *76*, 1665−1671.
(2) Slack, G. A. *CRC Handbook of Thermoelectrics*; Rowe, D. M., Ed.; CRC Press, 1995; pp 407−440.
(3) Mori, T.; Priya, S. Materials for energy harvesting: At the forefront of a new wave. *MRS Bull.* **2018**, *43*, 176−180.
(4) Petsagkourakis, I.; Tybrandt, K.; Crispin, X.; Ohkubo, I.; Satoh, N.; Mori, T. Thermoelectric materials and applications for energy harvesting power generation. *Sci. Technol. Adv. Mater.* **2018**, *19*, 836−862.
(5) Shirotani, I.; Uchiumi, T.; Ohno, K.; Sekine, C.; Nakazawa, Y.; Kanoda, K.; Todo, S.; Yagi, T. handbook on the physics and chemistry of rare earth. *Phys. Rev. B* **1997**, *56*, 7866.
(6) Uchiumi, T.; Shirotani, I.; Sekine, C.; Todo, S.; Yagi, T.; Nakazawa, Y.; Kanoda, K. Superconductivity of LaRu4X12 (X= P, As and Sb) with skutterudite structure. *J. Phys. Chem. Solids* **1999**, *60*, 689.
(7) Bauer, E. D.; Frederick, N. A.; Ho, P.-C.; Zapf, V. S.; Maple, M. B. *Phys. Rev. B* **2002**, *65*, No. 100506.
(8) Meisner, G. P.; Torikachvili, M. S.; Yang, K. N.; Maple, M. B.; Guertin, R. P. Properties and Applications of Thermoelectric Materials. *J. Appl. Phys.* **1985**, *57*, 3073.
(9) Shirotani, I.; Uchiumi, T.; Sekine, C.; Kimura, S.; Hamaya, N. Science and Technology of High Pressure. *J. Solid State Chem.* **1999**, *142*, 146.
(10) Torikachvili, M. S.; Rossel, C.; McElfresh, M. W.; Maple, M. B.; Guertin, R. P.; Meisner, G. P. Superconductivity, Heavy Fermion Behavior, and Crystalline Electric Field Effects in the Filled Skutterudite Series Pr (Os_1_-x_RUx_)_4Sb_1_2. *J. Magn. Magn. Mater.* **1986**, *54*, 365.
(11) Danebrock, M. E.; Evers, C. B. H.; Jeitschko, W. Proceedings ICT. *J. Phys. Chem. Solids* **1996**, *57*, 381.
(12) Keller, L.; Fischer, P.; Herrmannsdörfer, T.; Dönni, A.; Sug awara, H.; Matsuda, T. D.; Abe, K.; Aoki, Y.; Sato, H. Structural and magnetic properties of RFe4P12 (R= Pr, Nd) studied by neutron diffraction. *J. Alloys Compd.* **2001**, *323*, 516.
(13) Tenya, K.; Oeschler, N.; Gegenwart, P.; Steglich, F.; Frederick, N. A.; Bauer, E. D.; Maple, M. B. Acta Low-temperature magnetization of the skutterudite superconductor. *Phys. Polym. B* **2003**, *34*, 995.
(14) Sekine, C.; Uchiumi, T.; Shirotani, I.; Matsuhira, K.; Sakakibara, T.; Goto, T.; Yagi, T. Magnetic properties of the filled skutterudite-type structure compounds GdRu4P12 and TbRu4P12 synthesized under high-pressure. *Phys. Rev. B* **2000**, *62*, 11581.
(15) Dordevic, S. V.; Basov, D. N.; Dilley, N. R.; Bauer, E. D.; Maple, M. B. Hybridization gap in heavy fermion compounds. *Phys. Rev. Lett.* **2001**, *86*, 684.
(16) Yamasaki, A.; Imada, S.; Masuda, T.; Nanba, T.; Sekiyama, A.; Sugawara, H.; Matsuda, T. D.; Sato, H.; Sekine, C.; Shirotani, I.; Harima, H.; Suga, S. Heavy Fermion Behavior of Pr 4f Electrons in Filled Skutterudites Studied by Bulk-Sensitive Photoemission. *Acta Phys. Polym., B* **2003**, *34*, 1035.
(17) Bauer, E. D.; Slebarski, A.; Freeman, E. J.; Sirvent, C.; Maple, M. B. Kondo insulating behavior in the filled skutterudite compound CeOs4Sb12. *J. Phys.: Condens. Matter* **2001**, *13*, 4495.
(18) Sekine, C.; Uchiumi, T.; Shirotani, I.; Yagi, T. Metal-insulator transition in PrRu4P12 with skutterudite structure. *Phys. Rev. Lett.* **1997**, *79*, 3218.
(19) Blaha, P.; Schwarz, K.; Madsen, G. K. H.; Kvasnicka, D.; Luitz, J. *WIEN2k, An Augmented Plane Wave+Local Orbitals Program for Calculating Crystal Properties*; Schwarz, K., Ed.; Techn. Universitaet Wien: Wien, Austria, 2001.
(20) Blaha, P.; Schwarz, K.; Sorantin, P.; Trickey, S. B. Full-potential, linearized augmented plane wave programs for crystalline systems. *Comput. Phys. Commun.* **1990**, *59*, 399.
(21) Perdew, J. P.; Burke, K.; Ernzerhof, M. Generalized Gradient Approximation Made Simple. *Phys. Rev. Lett.* **1996**, *77*, 3865.
(22) Tran, F.; Blaha, P. Accurate Band Gaps of Semiconductors and Insulators with a Semilocal Exchange−Correlation Potential. *Phys. Rev. Lett.* **2009**, *102*, 226401.
(23) Dudarev, S. L.; Botton, G. A.; Savrasov, S. Y.; Humphreys, C. J.; Sutton, A. P. Electron-energy-loss spectra, and the structural stability of nickel oxide: An LSDA+U study. *Phys. Rev. B* **1998**, *57*, 1505.
(24) Madsen, G. K.; Singh, D. J.; et al. BoltzTraP. A code for calculating band-structure dependent quantities. *Comput. Phys. Commun.* **2006**, *175*, 67.
(25) Singh, D. J. Doping-dependent thermopower of PbTe from Boltzmann transport calculations. *Phys. Rev. B* **2010**, *81*, No. 195217.
(26) Marx, D.; Hutter, J. *Ab-initio Molecular Dynamics: Basic Theory and Advanced Methods*; Cambridge University Press, 2009.
(27) Bainsla, L.; Mallick, A. I.; Coelho, A. A.; Nigam, A. K.; Varaprasad, B. S.; Takahashi, Y. K.; Alam, A.; Suresh, K. G.; Hono, K. High spin polarization and spin splitting in equiatomic quaternary CoFeCrAl Heusler alloy. *J. Magn. Magn. Mater.* **2015**, *394*, 394.
(28) Birch, F. Finite strain isotherm and velocities for single-crystal and polycrystalline NaCl at high pressures and 300 K. *J. Geophys. Res.* **1978**, *83*, 1257.
(29) Shirotani, I.; Noro, T.; Hayashi, J.; Sekine, C.; Giri, R.; Kikegawa, T. X-ray study with synchrotron radiation for P-and Sb-based skutterudite compounds at high pressures. *J. Phys.: Condens. Matter* **2004**, *16*, 16.
(30) Ahmad Khandy, S.; Chai, J. D. Robust stability, half-metallic ferrimagnetism, and thermoelectric properties of new quaternary Heusler material: A first principles approach. *J. Magn. Magn. Mater.* **2020**, *502*, 166562.
(31) Dar, S. A.; Sharma, R.; Srivastava, V.; Sakalle, U. K. Investigation on the electronic structure, optical, elastic, mechanical, thermodynamic, and thermoelectric properties of wide band gap semiconductor double perovskite Ba2InTaO 6. *RSC Adv.* **2019**, *9* (17), 9522−9532.
(32) Li, X. G.; Liu, W. D.; Li, S. M.; Li, D.; Zhu, J. X.; Feng, Z. Y.; Chen, Z. G.; et al. Ce filling limit and its influence on the thermoelectric performance of Fe3CoSb12-based skutterudite grown by a temperature gradient zone melting method. *Materials* **2021**, *14* (22), 6810.
(33) Qiu, P. F.; Yang, J.; Liu, R. H.; Shi, X.; Huang, X. Y.; Snyder, G. J.; Zhang, W.; Chen, L. D. High-temperature electrical and thermal transport properties of fully filled skutterudites RFe4Sb12 (R= Ca, Sr, Ba, La, Ce, Pr, Nd, Eu, and Yb). *J. Appl. Phys.* **2011**, *109* (6), 063713.
(34) Kihou, K.; Shirotani, I.; Shimaya, Y.; Sekine, C.; Yagi, T. High-pressure synthesis, electrical and magnetic properties of new filled skutterudites LnOs4P12 (Ln= Eu, Gd, Tb, Dy, Ho, Y). *Mater. Res. Bull.* **2004**, *39* (2), 317−325.
(35) Awaji, K.; Nakajima, R.; Nishimura, K.; Takedachi, T.; Ando, T.; Kawamura, Y.; Sekine, C. High-Pressure Synthesis and Thermo-

electric Properties of Partially Filled Skutterudites RxCo4Sb12 (R= In, Tb and Dy). *Mater. Lett.* **2022**, *63* (6), 776−782.
(36) Trivedi, V.; Battabyal, M.; Balasubramanian, P.; Muralikrishna, G. M.; Jain, P. K.; Gopalan, R. (2018). Microstructure and doping effect on the enhancement of the thermoelectric properties of Ni doped Dy filled CoSb 3 skutterudites. *Sustainable Energy Fuels* **2018**, *2* (12), 2687−2697.
(37) Wei, X. P.; Sun, W.; Zhang, Y. L.; Sun, X. W.; Song, T.; Wang, T.; Zhu, X. F. (2017). Investigations on electronic, Fermi surface, Curie temperature and optical properties of Zr2CoAl. *J. Solid State Chem.* **2017**, *247*, 97−104.
(38) Yan, P. L.; Zhang, J. M.; Zhou, B.; Xu, K. W. The structural, electronic, magnetic, and mechanical properties of quaternary Heusler alloys ZrTiCrZ (Z= Al, Ga, In, Si, Ge, Sn): a first-principles study. *J. Phys. D: Appl. Phys.* **2016**, *49* (25), 255002.
(39) Gotoh, H.; Takeda, Y.; Asano, H.; Zhong, J.; Rajinikanth, A.; Hono, K. Spintronics, superconductivity, and strongly correlated materials-Antiferromagnetism and Spin Polarization in Double Perovskite $SrLaVMoO_6$. *Appl. Phys. Express* **2009**, *2*, No. 013001.
(40) Blundell, S. *Magnetism in Condensed Matter*; Oxford University Press, 2001; pp 94−95.
(41) Jamal, M. Cubic-Elastic, 2019. http://www.WIEN2k.at/reg_user/unsupported/cubic-elast/.
(42) Khandy, S. A.; Yousuf, S.; Gupta, D. C. Structural, Magneto-electronic, Mechanical, and Thermophysical Properties of Double Perovskite Ba2ZnReO6. *Phys. Status Solidi B* **2019**, *256*, No. 1800625.
(43) Benkaddour, K.; Chahed, A.; Amar, A.; Rozale, H.; Lakdja, A.; Benhelal, O.; Sayede, A. (2016). First-principles study of structural, elastic, thermodynamic, electronic, and magnetic properties for the quaternary Heusler alloys CoRuFeZ (Z= Si, Ge, Sn). *J. Alloys Compd.* **2016**, *687*, 211−220.
(44) Pugh, S. F. London, Edinburgh Dublin Philos., Relations between the elastic moduli and the plastic properties of polycrystalline pure metals. *Mag. J. Sci.* **1954**, *45*, 823.
(45) Kaur, K.; Kumar, R. Ti-based half Heusler compounds: a new on the screen with robust thermoelectric performance. *J. Alloys Compd.* **2017**, *727*, 1171−1177.
(46) Kaur, K.; Kumar, R. Giant thermoelectric performance of novel TaIrSn Half Heusler compound. *Phys. Lett. A* **2017**, *381* (44), 3760−3765.
(47) Khandy, S. A.; Gupta, D. C. Intrinsic magnetism, and thermoelectric applicability of novel halide perovskites Cs2GeMnX6 (X= Cl, Br): Route towards spintronics and energy harvesting technologies. *Mater. Sci. Eng., B* **2021**, *265*, No. 114985.
(48) Fine, M. E.; Brown, L. D.; Marcus, H. L. Elastic constants versus melting temperature in metals. *Scr. Metall.* **1984**, *18* (9), 951−956.
(49) Petit, A. T.; Dulong, P. L. Study on the measurement of specific heat of solids. *Ann. Chim. Phys.* **1819**, *55* (3), 240−246.
(50) Madsen; Singh, D. J.; et al. BoltzTraP. A code for calculating band-structure dependent quantities. *Comput. Phys. Commun.* **2006**, *175* (1), 67−71.

https://doi.org/10.1021/acsomega.3c06694
ACS Omega 2023, 8, 48113−48129